Level structure in the transitional nucleus ^{199}Tl

C. B. Li (李聪博),[1,*] X. G. Wu (吴晓光),[1,†] Y. Zheng (郑云),[1] Y. J. Jin (金彦君),[1,2] H. L. Ma (马海亮),[1] G. S. Li (李广生),[1] J. Zhong (钟健),[1] B. J. Zhu (朱保吉),[1] T. X. Li (李天晓),[1,3] Y. X. Gao (高彦祥),[1] X. Guan (管弦),[4] and J. Q. Liu (刘佳强)[4]

[1]*China Institute of Atomic Energy, Beijing 102413, China*

[2]*College of Physics and Technology, Shenzhen University, Shenzhen 518060, China*

[3]*Shenyang Institute of Engineering, Shenyang 110136, China*

[4]*College of Physics, Jilin University, Changchun 130012, China*

(Received 8 November 2017; revised manuscript received 22 February 2018; published 30 March 2018)

High-spin level structures of ^{199}Tl have been studied by in-beam γ-ray spectroscopic methods using the ^{196}Pt(^{7}Li, $4n$)^{199}Tl reaction at 40 MeV of beam energy. A large number of new states have been found, resulting in a significant extension of the previously known level scheme with the observation of 44 new transitions and 33 new levels. By comparing with the level structures in the odd-mass Tl isotopes and the even-even core Hg nuclei, configurations are proposed for the newly observed rotational bands and states in ^{199}Tl. The properties of the strongly coupled positive- and negative-parity bands can be interpreted in terms of the cranked Nilsson-Strutinsky-Bogoliubov model calculations, which show that the observed bands are built on the oblate shapes.

DOI: 10.1103/PhysRevC.97.034331

I. INTRODUCTION

The thallium isotopes ($Z = 81$) provide a rich laboratory for the study of nuclear shapes and have attracted considerable experimental and theoretical attention in the last few decades [1–4]. In spite of the location adjacent to a closed shell number of protons, the states observed to occur in these isotopes reveal an impressive variety of excitations built on different shapes, spherical, prolate, oblate, and triaxial, as well as normal and superdeformed [5–37]. The properties of these various modes of excitation present challenges to nuclear models and spur interest in understanding the configurations involved.

In odd-mass Tl ($Z = 81$) isotopes, the spin parity of $1/2^+$ for the ground states could be understood as being due to the $\pi 3s_{1/2}$ proton-hole orbital. The known $9/2^-$ isomer states have been shown to arise from the oblate minimum [38–40], and, where seen, the rotational bands built on the $9/2^-$ states have properties consistent with the $9/2^-[505]$ orbital from the oblate shape [5–7]. Later, rotational bands associated with both oblate ($\pi h_{9/2}$, $\pi i_{13/2}$) and prolate ($\pi h_{9/2}$, $\pi i_{13/2}$, $\pi f_{7/2}$) structures have been also observed in light Tl isotopes including the superdeformed structure in deficient neutron $^{189-195}$Tl [30–33]. While slightly oblate shapes dominate the low-energy structure of heavy Tl nuclei ($A > 189$) [12,25], prolate shapes are lower in energy for the lighter isotopes. However, as the neutron number increases, the levels in heavy ^{201}Tl become somewhat irregular and more spherical in nature, although the collective rotational nature of the $9/2^-$ band for the ^{201}Tl isotope still persists [41]. As one moves subsequently toward the $N = 126$ shell closure, the absence of any regular bandlike structure for the low-lying states in the heavier odd-mass Tl isotopes suggests spherical shapes for these nuclei at low excitation energy. Moreover, noncollective prolate shape ($\gamma = -120^\circ$) in this region has been invoked to account for the existence of irregular sequences observed in ^{193}Tl [13]. Very recently, a possible chiral band structure associated with triaxial deformation has also been reported at high excitation beyond first band crossing in ^{193}Tl [37,42].

The odd-mass nucleus ^{199}Tl, with the neutron number $N = 118$, is an interesting transitional nucleus whose two immediate odd-mass neighbors on either side have different shapes. As mentioned above, the spherical shape dominates in the heavier ^{203}Tl [43] and the deformed shape dominates in ^{197}Tl [7,44]. Moreover, a recent study indicates that ^{201}Tl is best described as a transitional nucleus with a combination of collective and single-particle excitations [41]. Thus, a knowledge of the structure of ^{199}Tl should yield useful information to study systematically the change in nuclear structure and shapes in the shape-transition region. However, the present knowledge of ^{199}Tl is particularly limited. The level structures are known only up to the tentative $(15/2^-)$ and $(15/2^+)$ states, respectively. Clearly, more spectroscopic information is needed on ^{199}Tl to obtain a high-spin level scheme as rich as that in ^{201}Tl and other lighter odd-mass Tl isotopes.

The results presented here extend considerably the level schemes obtained in earlier work. Several level sequences have been identified for the first time and the negative-parity yrast band structures established previously have been extended to higher spins beyond band crossing. Remarkable similarities as well as some notable differences have been found with the level structures of lighter odd-mass Tl isotopes. Coupling of an unpaired proton to the ^{198}Hg core is debated and used for the description of majority of these bands or states. At the same time, the cranked Nilsson-Strutinsky-Bogoliubov (CNSB) calculations to understand the observed properties are also presented.

*Corresponding author: licb@ciae.ac.cn

†Corresponding author: wxg@ciae.ac.cn

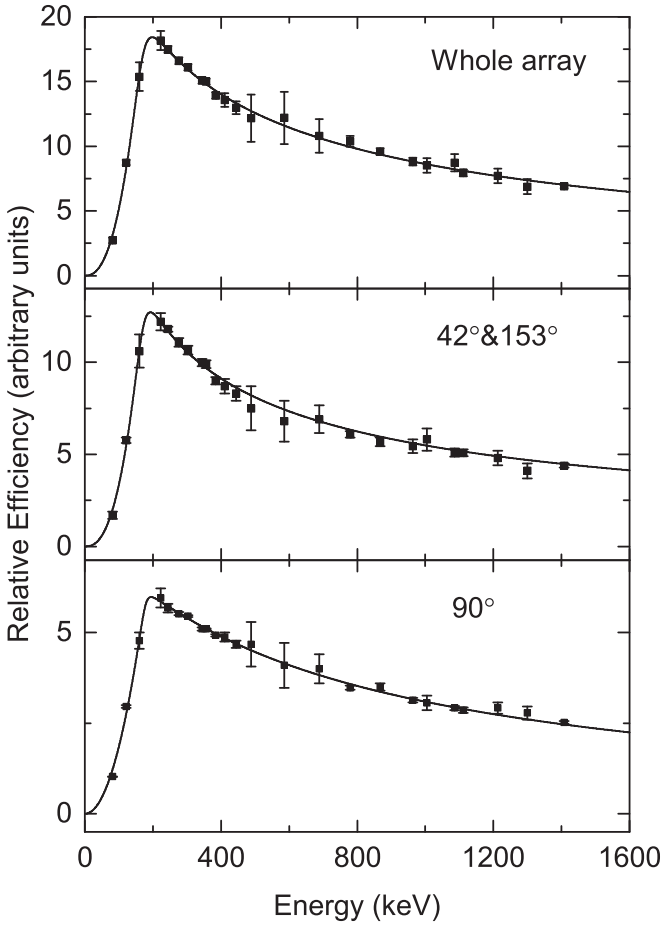

FIG. 1. Relative efficiencies of the CIAE detector array. Top: Whole array. Middle: 42° and 153° detectors. Bottom: 90° detectors.

II. EXPERIMENT

In the present experiment, excited states in ^{199}Tl were populated using the fusion evaporation reaction ^{196}Pt(^{7}Li, $4n$)^{199}Tl at an incident beam energy of 40 MeV. The ^{7}Li beam was delivered by the HI-13 tandem accelerator at the China Institute of Atomic Energy (CIAE). The target consisted of a 1.22 mg/cm^2 self-supporting foil of enriched ^{196}Pt with 94.57% enrichment. The deexcitation γ rays from the reaction residues were detected with an array consisting of eight Compton-suppressed HPGe detectors and two planar HPGe detectors, which were kept at 42° (one), 90° (four), and 153° (five) with respect to the beam direction. The relative photo-peak efficiency of the detector array and energy calibration were performed using the standard ^{152}Eu and ^{133}Ba radioactive sources. The efficiencies as a function of energy in our experiment are shown in Fig. 1, which can be achieved by fitting the data points using the following parametrization [45]

$$\ln(\epsilon) = [(A + Bx + Cx^2)^{-G} + (D + Ey + Fy^2)^{-G}]^{-1/G}, \quad (1)$$

where ϵ is the efficiency, $x = \ln(E_\gamma/100)$ and $y = \ln(E_\gamma/1000)$. The γ-ray energy E_γ is in keV. A, B, and C are the fit parameters for the low-energy region and D, E, and F are the fit parameters for the high-energy region. The G parameter determines the shape of the turnover region between the high- and low-energy efficiency curves.

A total of 36×10^6 γ-γ twofold and higher coincidence events were recorded. The data were sorted into symmetrized and angular correlation γ-γ matrices for off-line analysis. An asymmetric angular correlation matrix between the detectors at forward and backward directions and at 90° was constructed and used for the directional correlation of oriented states (DCO) ratio analysis to distinguish between quadrupole and dipole transitions. In our array geometry, a DCO ratio of about 1.0 is expected if the gating and the observed transition are stretched transitions of pure and equal multipole order. $R_{DCO} \approx 0.6$ is expected for a pure dipole transition gated on a stretched quadrupole transition. The inverse value of $R_{DCO} \approx 1.7$ is expected for a quadrupole transition gated on a dipole transition. Both ratios distinguish clearly between stretched dipole and quadrupole transitions whereas it is impossible to distinguish between stretched quadrupole and $\Delta I = 0$ transitions. The spin and parity assignments given in the present work follow from the previously established level assignments and the deduced multipolarities of newly observed transitions.

III. LEVEL SCHEME

Before this work only a few levels were known in ^{199}Tl. The first studies by Diamond and Stephens [47] and by Andersson *et al.* [48] had identified three excited states, including the $9/2^-$ metastable state with a half-life of 28.4 ms, built on the $1/2^+$ ground state. Afterward, Newton *et al.* [5] established a band built on the $9/2^-$ isomer with the $11/2^-$, $13/2^-$, and tentative $(15/2^-)$ states. They also assigned two possible positive-parity $(13/2^+)$ and $(15/2^+)$ states through 629 keV and 535 keV γ-rays transitions feeding the negative-parity $9/2^-$ band. Recently, Mărginean *et al.* [49] added a few new transitions to the two band structures built on the lowest $1/2^+$ and $3/2^+$ states using ^{197}Au$(\alpha, 2n)$ reaction. The present work, shown in Fig. 2, has extended the previous level scheme above the $9/2^-$ isomer with 44 new transitions and 33 new levels, consists of six sequences. The number labels are introduced to ease the discussion. Table I lists all transitions assigned to ^{199}Tl with their energies, intensities, DCO ratios, and assignments into the level scheme. It should be mentioned that the present experiments considerably only extend the level scheme above the $9/2^-$ isomer, but no more γ rays are observed feeding the $1/2^+$ ground state.

Band 1 previously known to $(15/2^-)$ has been extended to $(33/2^-)$ state with the observation of a sequence of new $\Delta I = 1$ transitions of 329, 466, 172, 226, 116, 112, 353, 266 keV and some of $\Delta I = 2$ crossover transitions of 746, 795, and 638 keV. Placement of these γ transitions were assigned from analysis of individual γ-γ coincidence spectra and their intensities. Further support for the placement of the γ rays within the band was derived from consideration of energy sums. Apparently, coincidence relations between $M1 + E2$ cascade and $E2$ crossover transitions give great confidence in the level scheme of the negative-parity states up to spin $21/2^-$. For higher spins, these $E2$ crossover transitions have

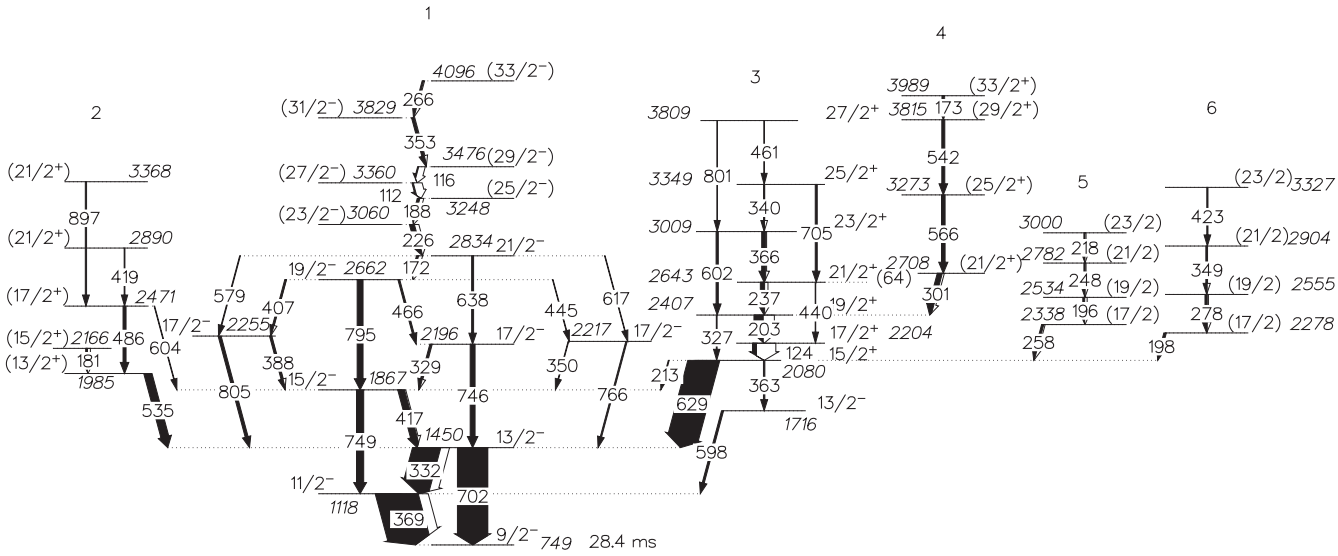

FIG. 2. Partial level scheme of ^{199}Tl obtained in the present work. The width of the arrows is proportional to the intensity of the transitions, while the white part of the arrows is the correction due to internal conversion [46]. The strongly populated states up to $I^{\pi} = 15/2^{-}$ are in agreement with previous work.

not been observed, the ordering was based on the intensities after accounting for appropriate internal conversion from Rösel *et al.* [46]. All new transitions added to band 1 are clearly displayed in the coincidence spectra gated on the 795 and 226 keV transitions, respectively [Figs. 3(a), 3(b)]. The 353 and 266 keV γ rays have been placed above the 112 and 116 keV lines in the level scheme of Fig. 2 based on the assumption that the latter two γ rays are strongly converted $M1 + E2$ transitions. However, the sequence ordering of these transitions still could not be determined unambiguously as the total intensities of the 112 and 116 keV lines could not be obtained due to the lack of any experimental information about the internal conversion coefficients. Two continuous low-energy transitions corresponding to the $27/2^{-} \rightarrow 25/2^{-}$ and $29/2^{-} \rightarrow 27/2^{-}$ transition have been found in ^{197}Tl [7]. Thus, the 112 and 116 keV γ rays have been tentatively assigned as the $(27/2^{-}) \rightarrow (25/2^{-})$ and $(29/2^{-}) \rightarrow (27/2^{-})$ transitions based on the systematic similarity of the level schemes of ^{197,199}Tl. An unusual feature of this structure is that there are three $17/2^{-}$ states, which are closely linked with the yrast band, one at the 2196 keV level, another one at the 2217 keV, the third one at 2255 keV level. The $17/2^{-}$ level at the lowest excitation energy of 2196 keV is adopted as part of this band.

Structure 2 consists of several transitions with irregular energy spacings. All the γ rays involved in this structure are clearly visible in the spectrum gated on the 535 keV transition, $(13/2^{+}) \rightarrow 13/2^{-}$ in Fig. 3(c). Initially, Newton *et al.* [5] tentatively identified the 1985 keV level as the $13/2^{+}$ state based on angular distribution and conversion coefficient measurements, incompletely excluding an alternative $17/2^{-}$ state. Thereafter, Liu *et al.* [50] revised the 1985 keV level as the $17/2^{-}$ state based on their angular distribution measurements. Our present data favor $13/2^{+}$ over $17/2^{-}$, because the DCO ratios of 535, 486, and 419 keV transitions in the present work suggest $\Delta I = 2$ or 0 character. An $E2$ character for the 535 keV transition would require $17/2^{-}$ for the spin of the 1985 keV level, which would lead to a $21/2^{-}$ spin of the 2471 keV level and a linking $M3$ transition for 604 keV transition. Since $M3$ is excluded, the $17/2^{-}$ and $21/2^{-}$ possibilities of 1985 keV and 2471 keV levels are not allowed. In addition, if one assumes the 1985 keV as the $I^{\pi} = 17/2^{-}$, the whole level structure would become yrast. This scenario is deemed to be unlikely, since the strongly coupled band 1 should be more favorably populated. All the above results indicate that the 535 keV γ ray is most likely $E1$ ($\Delta I = 0$) type rather than $E2$ one, and hence the spin and parity of the 1985 keV level is suggested as $(13/2^{+})$. This state continues further up in the irregular sequence with 181, 419, and 897 keV transitions. It noted that the 419 keV transition is close in energy to the strong 417 keV line, but the spectrum gated by the 535 keV γ ray [in Fig. 3(c)] clearly shows this transition without contamination. Additionally, transitions of 181 and 897 keV were placed in parallel with the 486 and 419 keV lines, respectively.

Bands 3, 4, 5, and 6 are completely new. Only three transitions (629, 598, and 363 keV) linking these bands to band 1 had been observed previously. The transitions in these bands are illustrated in Fig. 4(a), where spectra gated on the 629 keV transition is shown. In this gated spectrum, almost all transitions assigned to these side bands can be seen. The R_{DCO} value of 0.61(6) obtained for the 629 keV transition gated by the 702 keV known $E2$ transition indicates that it is a $\Delta I = 1$ dipole transition. Moreover, the $E1$ character of the 629 keV γ ray has been reported in Ref. [5] for this transition, and hence the spin and parity of the 2080 keV level is $15/2^{+}$.

Band 3 based on the $15/2^{+}$ state has been established up to $27/2^{+}$. A representative spectrum for band 2 obtained from a gate on the 237 keV transition is shown in Fig. 4(b). This gate indicates not only γ rays in band 3, but also those 629, 598, and 363 keV transitions that link band 3 into band 1. Decays from band 4 are also observed in this gate because of the possible 64 keV transition that feed the level directly above the gated γ ray (see discussion below). The 367 keV transition

TABLE I. Level excitation energy E_x, energies E_γ, relative intensities, DCO ratios, initial- and final-state spin parities, and multipolarities of γ-ray transitions assigned to ^{199}Tl in the present work.

E_x (keV)	E_γ (keV)	I_γ	R_{DCO}(D)[a]	R_{DCO}(Q)[b]	$I_i^\pi \rightarrow I_f^\pi$	Mult.
1117.9	369.3	100.0(45)	1.03(7)	0.67(5)	$11/2^- \rightarrow 9/2^-$	$M1+E2$
1450.3	332.4	65.8(38)	0.96(6)	0.96(9)	$13/2^- \rightarrow 11/2^-$	$M1+E2$
	701.9	72.1(69)	1.70(8)	0.98(10)	$13/2^- \rightarrow 9/2^-$	$E2$
1716.4	598.5	4.5(6)		1.00(11)	$13/2^- \rightarrow 11/2^-$	$M1+E2$
1867.1	416.8	15.9(11)		0.59(9)	$15/2^- \rightarrow 13/2^-$	$M1+E2$
	749.2	16.9(9)		0.94(17)	$15/2^- \rightarrow 11/2^-$	$E2$
1985.0	534.7	19.1(10)		1.19(13)	$(13/2^+) \rightarrow 13/2^-$	$E1$
2079.6	212.5	0.9(6)			$15/2^+ \rightarrow 15/2^-$	$E1$
	363.2	3.3(5)		1.19(13)	$15/2^+ \rightarrow 13/2^-$	$E1$
	629.3	74.0(28)		0.61(6)	$15/2^+ \rightarrow 13/2^-$	$E1$
2166.3	181.3	4.3(5)		0.56(10)	$(15/2^+) \rightarrow (13/2^+)$	$M1+E2$
2196.0	328.9	4.3(7)		0.57(17)	$17/2^- \rightarrow 15/2^-$	$M1+E2$
	745.7	9.1(13)		0.97(14)	$17/2^- \rightarrow 13/2^-$	$E2$
2203.6	124.0	9.6(13)	1.13(14)	0.67(12)	$17/2^+ \rightarrow 15/2^+$	$M1+E2$
2216.6	349.5	1.2(4)			$17/2^- \rightarrow 15/2^-$	$M1+E2$
	766.3	3.1(11)		1.03(16)	$17/2^- \rightarrow 13/2^-$	$E2$
2255.1	388.0	1.2(4)			$17/2^- \rightarrow 15/2^-$	$M1+E2$
	804.8	3.1(11)		0.88(19)	$17/2^- \rightarrow 13/2^-$	$E2$
2277.7	198.1	5.4(12)	1.32(21)	0.64(16)	$(17/2) \rightarrow 15/2^+$	
2338.0	258.4	5.1(5)	1.34(19)	0.64(9)	$(17/2) \rightarrow 15/2^+$	
2406.6	203.0	22.3(7)	0.99(10)	0.61(9)	$19/2^+ \rightarrow 17/2^+$	$M1+E2$
	327.0	1.7(4)	1.57(52)		$19/2^+ \rightarrow 15/2^+$	$E2$
2471.1	486.1	7.0(8)		1.12(11)	$(17/2^+) \rightarrow (13/2^+)$	$E2$
	604.0	1.4(12)			$(17/2^+) \rightarrow 15/2^-$	$E1$
2534.1	196.1	4.5(11)	1.28(33)	0.56(20)	$(19/2) \rightarrow (17/2)$	
2555.2	277.5	5.5(5)	1.23(21)	0.63(17)	$(19/2) \rightarrow (17/2)$	
2643.2	236.6	10.3(10)	1.17(14)	0.55(8)	$21/2^+ \rightarrow 19/2^+$	$M1+E2$
	439.6	1.2(4)	1.63(66)		$21/2^+ \rightarrow 17/2^+$	$E2$
2661.9	406.8	3.5(5)		0.69(17)	$19/2^- \rightarrow 17/2^-$	$M1+E2$
	445.3	1.4(6)			$19/2^- \rightarrow 17/2^-$	$M1+E2$
	465.9	3.8(5)		0.57(12)	$19/2^- \rightarrow 17/2^-$	$M1+E2$
	794.8	14.0(17)		1.05(14)	$19/2^- \rightarrow 15/2^-$	$E2$
2707.6	301.0	11.7(10)	1.07(11)	0.56(8)	$(21/2^+) \rightarrow 19/2^+$	$M1+E2$
	(64.4)[c]				$(21/2^+) \rightarrow 21/2^+$	$M1$
2781.6	247.5	3.0(5)	1.04(15)	0.61(17)	$(21/2) \rightarrow (19/2)$	
2833.9	172.0	4.9(11)		0.55(12)	$21/2^- \rightarrow 19/2^-$	$M1+E2$
	578.8	2.1(5)	1.15(33)		$21/2^- \rightarrow 17/2^-$	$E2$
	617.3	1.6(7)			$21/2^- \rightarrow 17/2^-$	$E2$
	637.9	4.6(17)		1.15(13)	$21/2^- \rightarrow 17/2^-$	$E2$
2889.9	418.8	1.7(3)		1.15(18)	$(21/2^+) \rightarrow (17/2^+)$	$E2$
2904.5	349.3	3.2(4)	1.19(27)		$(21/2) \rightarrow (19/2)$	
2999.8	218.2	2.6(3)	1.07(14)		$(23/2) \rightarrow (21/2)$	
3008.7	365.5	9.5(10)	1.10(11)	0.64(11)	$23/2^+ \rightarrow 21/2^+$	$M1+E2$
	602.1	3.2(5)	1.45(25)	1.13(23)	$23/2^+ \rightarrow 19/2^+$	$E2$
3059.8	225.9	11.6(4)		0.67(13)	$(23/2^-) \rightarrow 21/2^-$	$M1+E2$
3248.0	188.2	7.3(4)		0.56(10)	$(25/2^-) \rightarrow (23/2^-)$	$M1+E2$
3273.3	565.7	8.4(7)	1.69(16)	0.96(18)	$(25/2^+) \rightarrow (21/2^+)$	$E2$
3327.4	422.9	3.7(4)	1.26(20)		$(23/2) \rightarrow (21/2)$	
3348.6	339.9	2.1(4)	0.93(20)		$25/2^+ \rightarrow 23/2^+$	$M1+E2$
	705.4	4.7(7)	1.60(28)	0.97(14)	$25/2^+ \rightarrow 21/2^+$	$E2$
3360.3	112.3	3.2(7)		0.70(15)	$(27/2^-) \rightarrow (25/2^-)$	$M1+E2$
3368.3	897.2	3.0(7)		0.93(16)	$(21/2^+) \rightarrow (17/2^+)$	$E2$
3476.1	116.1	2.6(6)		0.68(18)	$(29/2^-) \rightarrow (27/2^-)$	$M1+E2$
3809.4	460.8	0.9(4)	0.97(18)		$27/2^+ \rightarrow 25/2^+$	$M1+E2$
	800.7	0.9(2)	1.68(32)	1.08(35)	$27/2^+ \rightarrow 23/2^+$	$E2$
3815.2	541.9	7.0(8)	1.55(18)	0.88(20)	$(29/2^+) \rightarrow (25/2^+)$	$E2$
3829.1	352.7	6.0(7)		0.46(9)	$(31/2^-) \rightarrow (29/2^-)$	$M1+E2$

TABLE I. (*Continued.*)

E_x (keV)	E_γ (keV)	I_γ	R_{DCO}(D)[a]	R_{DCO}(Q)[b]	$I_i^\pi \rightarrow I_f^\pi$	Mult.
3988.6	173.4	3.8(10)	2.04(26)	1.14(11)	$(33/2^+) \rightarrow (29/2^+)$	$E2$
4095.6	266.5	3.6(7)		0.53(33)	$(33/2^-) \rightarrow (31/2^-)$	$M1+E2$

[a]From the 629 keV ($E1$) DCO gate.
[b]From the known quadrupole transition DCO gate.
[c]The transition energy is determined by the difference of the initial and final level energies.

$(3/2^+ \rightarrow 1/2^+)$ is the well-known ground-state transition in ^{199}Tl, which is in coincidence with the 382 keV transition $(9/2^- \rightarrow 3/2^+)$ deexciting the $9/2^-$ isomeric state (not plotted in Fig. 2). The other component of this wide multiplet 363 and 369 keV transitions are known to be the $15/2^+ \rightarrow 13/2^-$ and $11/2^- \rightarrow 9/2^-$ transitions, respectively. From the fact that a near 367 keV line is still present in the 629 and 237 keV transitions gates [shown in Figs. 4(a), 4(b)] and considering that the 629 and 237 keV transitions are not in coincident with 367 keV transition because of the long half-life of the $9/2^-$ isomer, it can be concluded that another component must exist. Its energy can be resolved through coincidence spectra. The gated spectrum of 382 keV transition shows the 367 keV line [shown in Fig. 5(a)], while the gated spectrum of 702 keV transition [shown in Fig. 5(b)] shows the 366 keV line, slightly lower in energy than the one in Fig. 5(a) (due to the contamination of 705 keV, the 369 keV peak is still seen in 702 keV gated spectrum). This component of 366 keV transition has been placed as the $23/2^+ \rightarrow 21/2^+$ transition. Analysis of the DCO ratios indicate that the transitions with $E_\gamma = 124$, 203, 237, 366, 340, 461 keV and the crossover transitions with $E_\gamma = 327$, 440, 602, 705, and 801 keV are consistent with stretched $\Delta I = 1$ and $\Delta I = 2$ transitions, respectively. The level ordering as well as the spin and parity assignments based on the $15/2^+$ state are rather firmly established because coincidence relations between cascade and crossover transitions yielded a powerful tool to place γ lines within the band. Furthermore, the coincidence intensity balance favors $M1$ multipolarity for the $\Delta I = 1$ transitions, as the low-energy γ rays are highly converted.

Band 4 is newly observed and consists of four levels with three irregular transitions of $E2$ nature. The 301 keV gated coincidence spectrum displayed in Fig. 4(c) clearly shows the all the three in-band transitions and 124, 203, and 327 keV transitions in band 3, but not seen in coincidence with the other transitions in band 3. A gate on the 237 keV transition [Fig. 4(b)] also reveals three transitions in band 4 notwithstanding weak intensities, but not in coincidence with the 301 keV transition. It must be concluded that the 301 keV dipole transitions parallel to the 237 keV transition and obtain a 21/2 state at 2708 keV. Furthermore, this establishes the presence of a connecting transition of 64 keV between the 2643 keV and the 2708 keV levels. However, it could not be seen because it has high internal conversion coefficient and it lies too close to the strong 65 keV x ray in the Pt target. The spins of band 4 are assigned using the DCO ratios measurements. However, band 4 is a structure observed for the first time, and no similar structures have been seen in

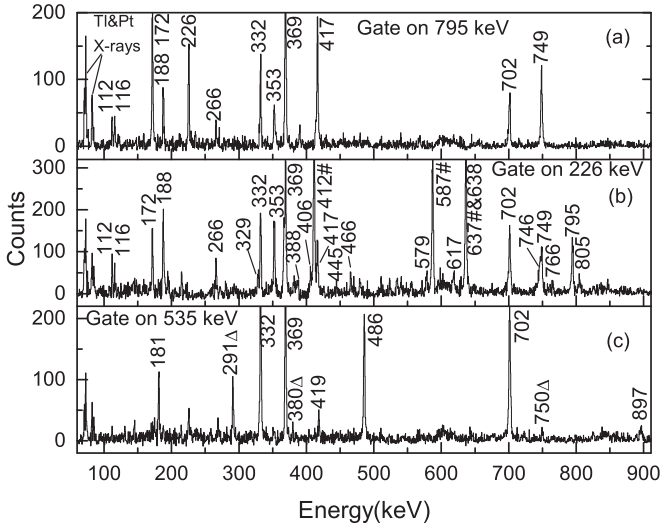

FIG. 3. γ-ray coincidence spectra for ^{199}Tl gated (a) on the 795 keV $(19/2^- \rightarrow 15/2^-)$, (b) on the 226 keV $[(23/2)^- \rightarrow (21/2^-)]$, and (c) on the 535 keV $[(13/2)^+ \rightarrow 13/2^-]$ transition. γ-ray lines denoted by # in the 226 keV gate and Δ in the 535 keV gate are those belonging to ^{198}Hg and ^{199}Hg from incomplete fusion channels, respectively.

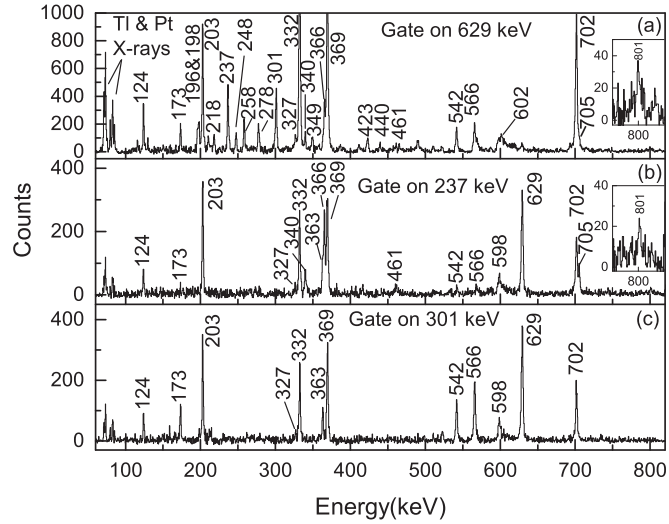

FIG. 4. γ-ray coincidence spectra for ^{199}Tl gated on the (a) 629 keV $(15/2^+ \rightarrow 13/2^-)$, (b) 237 keV $(21/2^+ \rightarrow 19/2^+)$, and (c) 301 keV $[(21/2^+) \rightarrow 19/2^+]$ transition. The insets in (a) and (b) show an expanded region around 800 keV.

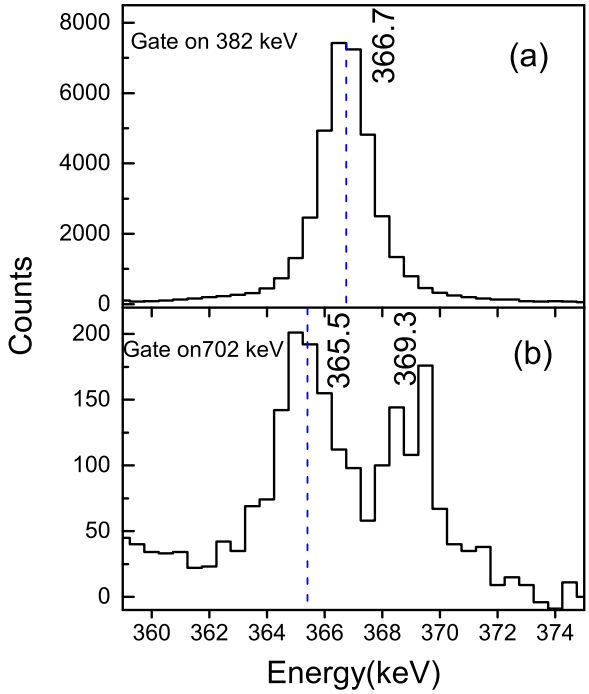

FIG. 5. γ-ray coincidence spectra for ^{199}Tl gated (a) on the 382 keV ($9/2^- \rightarrow 3/2^+$), (b) on the 702 keV ($13/2^- \rightarrow 9/2^-$) transition. The peak positions of the 365.5 keV and 366.7 keV γ-ray transitions are indicated with blue dash line.

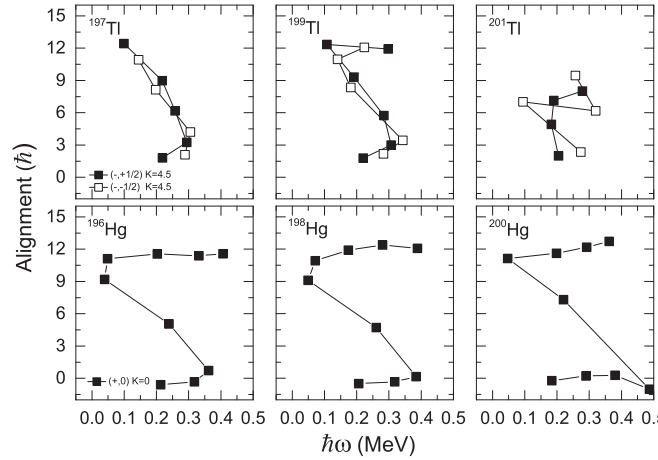

FIG. 6. Experimental alignments for the negative-parity oblate band structures in ^{197}Tl, ^{199}Tl, and ^{201}Tl (based on $9/2^-[505]$ configuration) and the yrast bands in their respective Hg core nuclei. The Harris reference parameters are chosen to be $J_0 = 8.0\hbar^2$ MeV^{-1} and $J_1 = 40.0\hbar^4$ MeV^{-3}.

any of the neighboring odd-mass Tl nuclei. Thus, possible parity assignment is not permitted to follow the systematic consideration. However, only tentatively, the parity of this band is proposed as positive based on likely configuration presented in the next section.

Besides the main decay path, two other sequences (5 and 6) are weakly populated and both feed the positive-parity $15/2^+$ state. These transitions are clearly visible in the coincidence spectrum gated on the 629 keV γ ray in Fig. 4(a). Their ordering is based on the measured intensities. The spin assignments are guided by DCO ratios, but no parity assignments have been made.

IV. DISCUSSION

Preliminary configuration of the low spin band 1 in ^{199}Tl was assigned as the $\pi h_{9/2}$ orbital ($9/2^-[505]$) coupled to the oblate ground state of the ^{198}Hg core, in analogy to the states in neighboring odd-mass Tl nuclei above the $9/2^-$ isomer. In the present extended level scheme, the energy spacings along this band start to compress at spin around $19/2^-$, clearly reflecting an intersection with a band consisting of three quasiparticles. To identify the active orbital involved, the experimental alignments for the negative-parity oblate band structures in the odd-mass $^{197-201}$Tl and the yrast bands in their respective Hg core nuclei were plotted in Fig. 6. In the even-even $^{196-200}$Tl [51–54] and the neighboring odd-mass ^{197,201}Tl [41,44], the $i_{13/2}$ neutron pair undergoes a rotational alignment at a close crossing frequency. It can be seen from Fig. 6 that the gains in alignment in ^{199}Tl is similar to the lighter ^{197}Tl and its ^{198}Hg core. The observed band crossing frequencies of ~0.30 MeV as well as the angular momentum gain of ~10.5$\hbar$ for band 1 in ^{199}Tl are in agreement with $\nu(i_{13/2})^2$ excitations. On the other hand, the neutron $i_{13/2}$ crossings occur much lower in frequency than the alternative proton $h_{11/2}$ alignment, which is expected to occur at a much higher rotational frequency of above 0.4 MeV [53,55–57]. It can therefore be concluded that the observed part of the band 1 above the band crossing is assigned as the $\pi h_{9/2} \otimes \nu i^2_{13/2}$ configuration.

Interestingly, as indicated by the alignment features from Fig. 6, one can see that ^{199}Tl behaves more like the neighboring lighter ^{197}Tl than the heavier ^{201}Tl. In the case of heavier ^{201}Tl, $\pi h_{9/2}$ band has a lower alignment gain. This indicates an abrupt change in the structure of the $9/2^-$ band in odd-mass Tl isotopes as the neutron number increases. An alternative neutron $f_{5/2}$ alignment cannot provide such large angular momentum; while more protons into the $h_{9/2}$ shell is suppressed by the large energy gap around $Z = 80$. Das Gupta *et al.* [41] describe the lower alignment as possibly being due to the partial alignment of $i_{13/2}$ neutron pair. Furthermore, the total Routhian surface (TRS) calculations in their work show that as the rotational frequency increases, the deformation gradually decreases and there is no minimum at the oblate shape and the deformation is close to $\beta_2 = 0$ above $\hbar\omega = 0.36$ MeV in ^{201}Tl. Therefore, the observation of the abnormal alignment gain in ^{201}Tl could be attributed to this shape or deformation change. In addition, the Tl isotopes alignment evolution trend seems to be different from the seen in their Hg cores, which well follow systematics. This indicates that the odd nucleon in ^{201}Tl itself may greatly affect the structure of the ^{200}Hg core.

In the present work, the strongly populated $13/2^+$ state at 1985 keV may be a candidate for the $\pi i_{13/2}$ state. Corresponding bands built upon this configuration have been observed in $^{183-193}$Tl [12–16,25,44,60]. However, the 13/2 state previously assigned positive parity in ^{193}Tl has been revised as

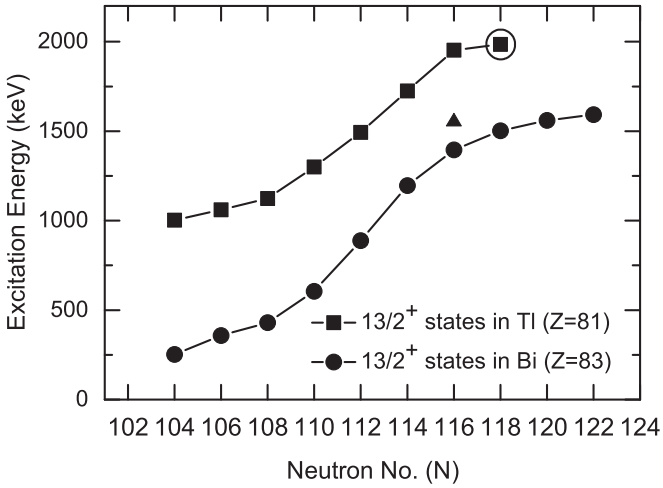

FIG. 7. Level energy systematics of the $13/2^+$ states in odd Tl and Bi isotopes as a function of neutron number. The encircled one corresponds to that in ^{199}Tl from the present work. The trigonal one corresponds to the suggested $13/2^+$ state in ^{197}Tl by H. Pai *et al.* [44,59].

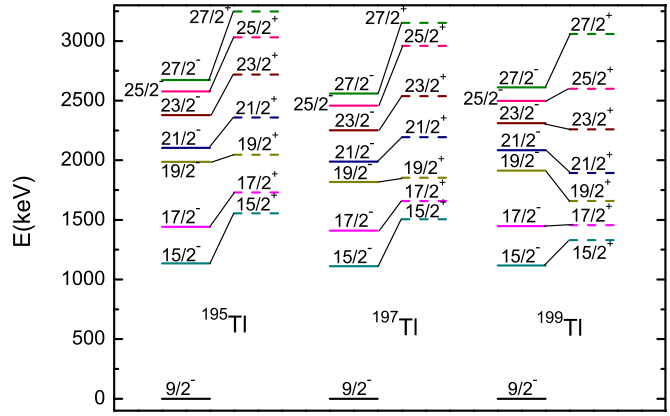

FIG. 8. Systematics of the excitation energy in the negative-parity yrast states and the positive-parity three-qp yrast states in odd-mass $^{195-199}$Tl.

negative parity through linear polarization measurements in very recent work [42]. In the heavier Tl isotopes, however, scarcity of the observation of γ transitions feeding the $13/2^+$ state makes it difficult to assign whether the $13/2^+[606]$ configuration to the structure was more rotational-like behavior or more single-particle character. For ^{199}Tl, the positive-parity branch (structure 2) based on the $13/2^+$ state does not appear to be collective in nature.

In a recent work [58], systematic studies of odd-mass neighboring Bi ($Z = 83$) nuclei show that sudden elevating of the $13/2^+$ level energies occurs as the neutron number increases (shown in Fig. 7), which has been attributed to the interaction of the $i_{13/2}$ proton with decreasing number of neutron holes. As can be easily seen in Fig. 7, the increase of the $i_{13/2}$ level energies is especially apparent for the $A = 191 - 199$ ($N = 108 - 116$) Bi isotopes. As approaching to the neutron $N = 126$ shell closure, this effect is less profound and the excitation energy of the $i_{13/2}$ state is observed to increase tends to saturate, suggesting near-spherical shapes for the heavier isotopes. The same investigation for the Tl isotopes is also shown in this figure for comparison. Apparently, the evolution of the energy of this state is very similar in Tl and Bi isotopes, which suggests that the above argument in Ref. [58] is also valid in neighboring odd-mass Tl isotopes. It should be noted that the suggested $13/2^+$ level by Pai *et al.* [44,59] (the trigonal sign in Fig. 7) does not follow the expected trend after addition the probable $13/2^+$ state in ^{195}Tl [60]. Therefore, we arbitrarily assumed the second $13/2^+$ states at 1953 keV in ^{197}Tl as a candidate for the $\pi i_{13/2}$ state. The systematic behavior of the $13/2^+$ levels supports the assumption that the 1985 keV level, tentatively assigned in the present work, is the proton $\pi[606]13/2^+$ intruder state. Notice, however, the decay path of the $13/2^+$ state in ^{199}Tl (a strong $E1$ transition feeding the $13/2^-$ state of $h_{9/2}$ band) is quite different from the cases in the lighter Tl isotopes, where a strong $E1$ transition feeding the $11/2^-$ state of $h_{9/2}$ band was observed.

The new band 3 is built above the $15/2^+$ state. It decays strongly toward band 1, and also toward the $13/2_2^-$ levels. This band has relatively high excitation energy (2080 keV) and spin, and thus is probably built on a three-quasiparticle (three-qp) configuration. A suitable configuration involving single-particle orbitals close to the Fermi level is $\pi h_{9/2} \otimes \nu i_{13/2} j$ (where $j = p_{3/2}, f_{5/2}, p_{1/2}$). This suggestion agrees well with the systematics, because in its neighboring odd-mass $^{193-197,201}$Tl [7,41,42,44] and their Hg cores configurations involving $\nu i_{13/2} j$ excitations were assigned to the lowest-energy bands involving two quasineutron excitations with negative parity. However, the three-qp band in ^{197}Tl has been modified to be of negative parity in Ref. [44], in contradiction to positive-parity assignment in a previous report [7].

From Fig. 8, one can see that the negative-parity yrast band is always more yrast than the positive parity three-qp $\pi h_{9/2} \otimes \nu i_{13/2} j$ band in the lighter odd-mass ^{195,197}Tl isotopes, which is different in the case of ^{199}Tl. Negative-parity band 1 in ^{199}Tl loses its yrast-band character between spins of $19/2 \leqslant I \leqslant 23/2$. In the above discussion, $19/2^-$ state has been mentioned as the start of rotational alignment of an $i_{13/2}$ neutron pair. It was argued in Refs. [52,54] that it is more economical to rearrange one $i_{13/2}$ neutron hole to a $(p_{3/2}, p_{1/2}, f_{5/2})$ orbital than excite an $i_{13/2}$ neutron pair when approaching the closure of $i_{13/2}$ for $N = 120$, and hence positive-parity band based on $\pi h_{9/2} \otimes \nu i_{13/2} j$ configuration decay path will be more favored to the ground-state band up to higher spins in ^{199}Tl. The effect of the $N = 120$ subshell closure was also observed in ^{198}Hg ($N = 118$) core, and more remarkable in heavier ^{200}Hg ($N = 120$), as expected. In addition, due to this effect of the shell closure, an additional $i_{13/2}$ neutron pair alignment above spin 15^- in corresponding $\nu i_{13/2} j$ band in ^{198,200}Hg core was observed resulting in a higher excitation energy than lighter even-even Hg isotopes [54], which is also expected in ^{199}Tl with $N = 118$ in the future experiment. However, for ^{201}Tl, the level scheme is very complex and do not well followed the level systematics because of the preceding discussed sudden structure change.

Band 4 has a sequence of successive $E2$ transitions, which decays into the three-qp $\pi h_{9/2} \otimes \nu i_{13/2} j$ band 3. Such a level

sequence for high spin states is a rather unique observation in heavy Tl isotopes. Here, we present a tentative interpretation of its structure. It seems from the level structure that the presence of only one signature indicates a low-K structure nature and the irregular spacing of the excitation energy levels is characteristic of oblate shape. Thus, we propose that this sequence is associated with the $h_{11/2}$ ($1/2^-[550]$) proton orbital at oblate deformation. The $(21/2^+)$, $(25/2^+)\ldots$ states observed in this band cloud be interpreted as the coupling of an $h_{11/2}$ proton to the 5^-, $7^-\ldots$ states in the ^{198}Hg core. The corresponding three-qp states with $I^\pi = 25/2^+$ have also been observed in the heavier ^{201,203,205}Tl isotopes [41,61,62]. However, no well-developed rotational band structure is observed in either of the nuclei.

The spins of bands 5 and 6 remain tentative and are not well developed. Therefore, characterization of these bands at this moment would be rather premature. However, the similarities in the values of excitation energy and spin with band 3 indicate that they are of similar configuration. In the neighboring odd-mass ^{197}Tl [44], two three-quasiparticle bands have been interpreted as $h_{9/2}$ or $i_{13/2}$ coupling the its Hg cores configurations involving $vi_{13/2}j$ excitations. Therefore, it appears that the bands 5 and 6 may be generated with $h_{9/2}$ or $i_{13/2}$ coupling the similar ^{198}Hg core configuration.

A. CNSB calculations

Two coupled bands 1 and 3 will be discussed within the framework of the cranked Nilsson-Strutinsky-Bogoliubov (CNSB) model [63,64] with pairing correlation included. In this approach, the total energy after the particle number projection, is minimized not only in deformation space but also in a mesh of the pairing parameters, Fermi energy λ, and paring gap Δ. Excellent agreement between the theoretical and the observed results in the low-spin regime has been reported for some of the nuclei [63,65–67]. Thus, one may expect that similar calculations for the low and intermediate states in ^{199}Tl may provide a good description of the observed structures in this nucleus.

The present CNSB calculation were carried out in a quadrupole and hexadecapole deformation mesh (ε_2, γ, ε_4) with the standard κ and μ parameters [68]. Total energies are calculated as the sum of the rotating liquid-drop energy (E_{rld}) and the shell energy using the Strutinsky method. The Lublin-Strasbourg drop (LSD) [69] model has been used for calculating the macroscopic energy, with the rigid-body moments of inertia calculated with a radius parameter of $r_0 = 1.16$ fm and a diffuseness of $a = 0.6$ fm. The total energy has been minimized at each spin in a deformation space spanned by the parameters ε_2, γ, ε_4.

The experimental and theoretical energies relative to a rotating liquid drop (rld) reference for the positive- and negative-parity bands in ^{199}Tl are plotted as a function of spin in Fig. 9. It is seen that the experimental data are generally reproduced, including the experimentally observed band crossing at spin $\sim 21/2^-$ in band 1. Selected examples of potential energy surfaces (PESs) for some states in the positive- and negative-parity yrast band are shown in Fig. 10. The calculations for the negative-parity bands with the configuration $(-,\pm 1/2)(+,0)$

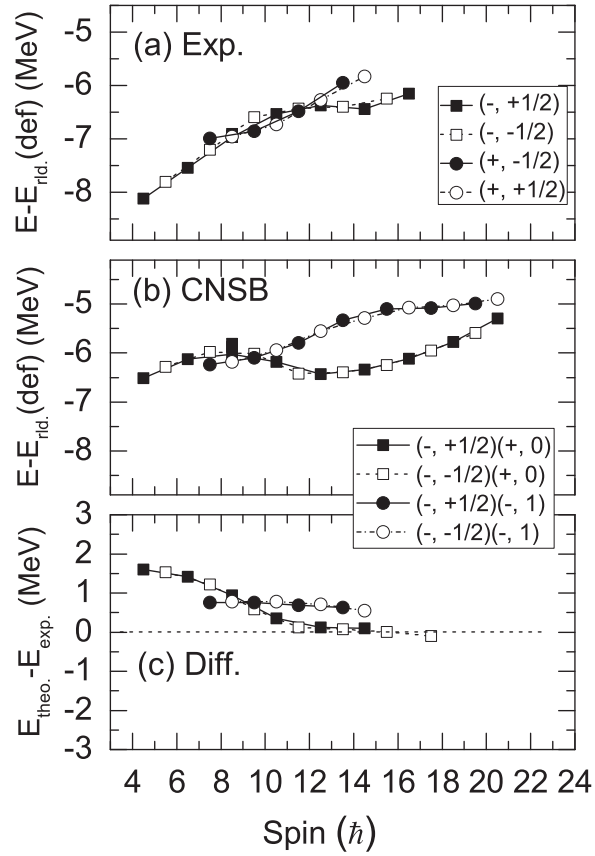

FIG. 9. The experimental and CNSB rotating energies in ^{199}T1. The theoretical bands are labeled by the combination of parity and signature of protons and neutrons $(\pi_p,\alpha_p)(\pi_n,\alpha_n)$.

and the positive-parity bands with the configuration $(-,\pm 1/2)(-,1)$ both show a minimum in the PESs at $\varepsilon_2 \sim 0.14$ and $\gamma \sim -60^\circ$, indicating oblate shapes. Therefore, the rotational bands observed in ^{199}Tl based on these configurations could provide a basis with oblate deformation, the same as that in the other lighter odd-mass Tl isotopes. There are several noncollective minima in the PESs with fewer particles excited, which are predicted to be more favored. However, no such states have been observed in the present experiment. The reason for this may lie in the fact that it is much easier to identify smooth collective structures that are close to the yrast line at high-spins where population occurs in fusion-evaporation reactions. For the spin $I^\pi = 17/2^-$ three competitive minima are present in the PES [shown in Fig. 10(a)] corresponding to collective oblate configuration ($\varepsilon_2 \sim 0.15, \gamma = -58^\circ$), aligned oblate noncollective configuration ($\varepsilon_2 \sim 0.14$, $\gamma = 60^\circ$), and slightly triaxial configuration ($\varepsilon_2 \sim 0.11$, $\gamma = 10^\circ$), respectively. The oblate noncollective and slightly triaxial states are 208 and 149 keV higher than the collective oblate state in the calculations, respectively. These states are also seen in the experimental level scheme and are 59 and 21 keV higher than that $17/2_1^+$ state.

The remaining question is in regard to the presence of chiral candidates, which have been suggested in ^{192,193,194}Tl [34,37,42], and also in the neighboring ^{198}Tl [23]. However, the

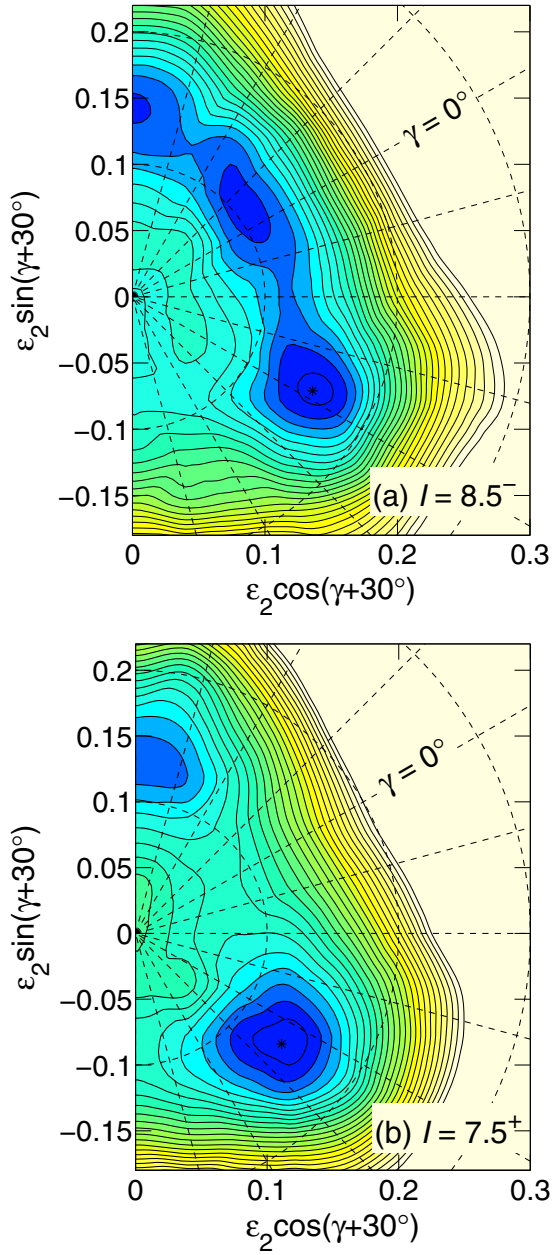

FIG. 10. Calculated potential energy surfaces for (a) $I^{\pi} = 17/2^{-}$ state of the $(-,1/2)(+,0)$ configuration; (b) $I^{\pi} = 15/2^{+}$ state of the $(-,1/2)(-,1)$ configuration. The contour line separation is 0.2 MeV.

present CNSB calculations do not yield a triaxial nuclear shape above band crossing spin in ^{199}Tl, and thus cannot support the presence of a chiral geometry in the angular momentum space. Furthermore, no observing signature splitting in the negative yrast band in ^{199}Tl agrees with this opinion.

V. SUMMARY

The present work has resulted in the placement of some 44 new γ rays and 33 new levels in the level scheme of ^{199}Tl. The strongly coupled rotational band built upon the $9/2^{-}$ isomer state has been extended beyond the particle alignment spins up to $(33/2^{-})$. Another strongly coupled band built on the coupling of a $h_{9/2}$ proton to the 5^{-} band of ^{198}Hg core was established up to the $27/2^{+}$. Further, a possible decoupled positive-parity band originating from the coupling of a low-K $h_{11/2}$ to the same core 5^{-} band was proposed. The $(13/2^{+})$ state at the excitation energy of 1985 keV has been proposed to originate from the occupation of the $\pi i_{13/2}$ $13/2^{+}[606]$ orbital based on the systematic of the energy of this state in the odd-mass Tl and neighboring Bi isotopes. The band structures are compared with the band structures in the other odd-mass Tl isotopes and also with their Hg cores. It has been observed that the remarkable similarity in the level structure of ^{199}Tl behaves more like the lighter neighboring odd-mass Tl isotopes than the heavier Tl isotopes. Two collective rotational coupled bands 1 and 3 are discussed within the framework of the cranked Nilsson-Strutinsky-Bogoliubov (CNSB) model with pairing correlation included. The excited energies and the band crossing in these bands are generally successful in providing a basis with oblate shape. Apparently, more experimental data is required on this and neighboring nuclei to help in making firmer configuration assignments and to understand fully the interaction between these competing structures and angular momentum mechanisms.

ACKNOWLEDGMENTS

The authors would like to thank the HI-13 tandem accelerator staff for the smooth operation of the machine. We are grateful to Dr. Q. W. Fan for his assistance during target preparation. This work is partially supported by the National Natural Science Foundation of China under Contracts No. 11375267, No. 11405274, No. 11475072, No. 11305269, and No. 11775307.

[1] K. Heyde, P. Van Isacker, M. Waroquier, J. L. Wood, and R. A. Meyer, Phys. Rep. **102**, 291 (1983).
[2] J. L. Wood, K. Heyde, W. Nazarewicz, M. Huyse, and P. V. Duppen, Phys. Rep. **215**, 101 (1992).
[3] K. Heyde and J. L. Wood, Rev. Mod. Phys. **83**, 1467 (2011).
[4] J. H. Hamilton, P. G. Hansen, and E. F. Zganjar, Rep. Prog. Phys. **48**, 631 (1985).
[5] J. O. Newton, S. D. Cirilov, F. S. Stephens, and R. M. Diamond, Nucl. Phys. A **148**, 593 (1970).
[6] J. O. Newton, F. S. Stephens, and R. M. Diamond, Nucl. Phys. A **236**, 225 (1974).
[7] R. M. Lieder *et al.*, Nucl. Phys. A **299**, 255 (1978).
[8] A. J. Kreiner, M. Fenzl, and W. Kutschera, Nucl. Phys. A **308**, 147 (1978).
[9] A. J. Kreiner, M. Fenzl, U. Heim, and W. Kutschera, Phys. Rev. C **20**, 2205 (1979).
[10] A. J. Kreiner, M. A. J. Mariscotti, C. Baktash, E. der Mateosian, and P. Thieberger, Phys. Rev. C **23**, 748 (1981).

[11] A. J. Kreiner, J. Davidson, M. Davidson, H. Mosca, L. L. Riedinger, C. R. Bingham, M. W. Guidry, and A. C. Kahler, Phys. Rev. C **38**, 2674 (1988).
[12] M. G. Porquet, A. J. Kreiner, F. Hannachi, V. Vanin, G. Bastin, C. Bourgeois, J. Davidson, M. Debray, G. Falcone, A. Korichi, H. Mosca, N. Perrin, H. Sergolle, F. A. Beck, and J. C. Merdinger, Phys. Rev. C **44**, 2445 (1991).
[13] W. Reviol *et al.*, Nucl. Phys. A **548**, 331 (1992).
[14] G. J. Lane, G. D. Dracoulis, A. E. Byrne, P. M. Walker, A. M. Baxter, J. A. Sheikh, and W. Nazarewicz, Phys. Lett. B **324**, 14 (1994).
[15] G. J. Lane, G. D. Dracoulis, A. E. Byrne, P. M. Walker, A. M. Baxter, J. A. Sheikh, and W. Nazarewicz, Nucl. Phys. A **586**, 316 (1995).
[16] M. Muikku, P. T. Greenlees, K. Hauschild, K. Helariutta, D. G. Jenkins, P. Jones, R. Julin, S. Juutinen, H. Kankaanpaa, N. S. Kelsall, H. Kettunen, P. Kuusiniemi, M. Leino, C. J. Moore, P. Nieminen, C. D. OLeary, R. D. Page, P. Rahkila, W. Reviol, M. J. Taylor, J. Uusitalo, and R. Wadsworth, Phys. Rev. C **64**, 044308 (2001).
[17] C. Y. Xie, X. H. Zhou, Y. H. Zhang, Y. X. Guo, X. G. Lei, Y. Zheng, M. L. Liu, L. T. Song, H. L. Wang, W. T. Guo, H. P. Yu, L. H. Zhu, X. G. Wu, and F. R. Xu, Phys. Rev. C **72**, 044302 (2005).
[18] S. K. Chamoli, P. Joshi, A. Kumar, R. Kumar, R. P. Singh, S. Muralither, R. K. Bhowmik, and I. M. Govil, Phys. Rev. C **71**, 054324 (2005).
[19] S. K. Chamoli, R. Kumar, I. M. Govil, P. Joshi, R. P. Singh, S. Muralithar, and R. K. Bhowmik, Phys. Rev. C **75**, 054323 (2007).
[20] H. Pai, G. Mukherjee, S. Bhattacharyya, M. R. Gohil, T. Bhattacharjee, C. Bhattacharya, R. Palit, S. Saha, J. Sethi, T. Trivedi, S. Thakur, B. S. Naidu, S. K. Jadav, R. Donthi, A. Goswami, and S. Chanda, Phys. Rev. C **85**, 064313 (2012).
[21] S. Bhattacharya *et al.*, Phys. Rev. C **95**, 014301 (2017).
[22] E. A. Lawrie, P. A. Vymers, J. J. Lawrie, C. Vieu, R. A. Bark, R. Lindsay, G. K. Mabala, S. M. Maliage, P. L. Masiteng, S. M. Mullins, S. H. T. Murray, I. Ragnarsson, T. M. Ramashidzha, C. Schuck, J. F. Sharpey-Schafer, and O. Shirinda, Phys. Rev. C **78**, 021305(R) (2008).
[23] E. A. Lawrie *et al.*, Phys. Eur. Phys. J. A **45**, 39 (2010).
[24] W. Reviol, L. L. Riedinger, J. Y. Zhang, C. R. Bingham, W. F. Mueller, B. E. Zimmerman, R. V. F. Janssens, M. P. Carpenter, I. Ahmad, I. G. Bearden, R. G. Henry, T. L. Khoo, T. Lauritsen, and Y. Liang, Phys. Rev. C **49**, 587(R) (1994).
[25] W. Reviol *et al.*, Phys. Scr., T **56**, 167 (1995).
[26] W. Reviol *et al.*, Nucl. Phys. A **630**, 434c (1998).
[27] S. M. Fischer, M. P. Carpenter, R. V. F. Janssens, B. Crowell, I. Ahmad, D. J. Blumenthal, T. L. Khoo, T. Lauritsen, D. Nisius, W. Reviol, W. F. Mueller, L. L. Riedinger, B. H. Smith, and B. Cederwall, Phys. Rev. C **53**, 2126 (1996).
[28] Y. Liang, M. P. Carpenter, R. V. F. Janssens, I. Ahmad, R. G. Henry, T. L. Khoo, T. Lauritsen, F. Soramel, S. Pilotte, J. M. Lewis, L. L. Riedinger, C. H. Yu, U. Garg, W. Reviol, and I. G. Bearden, Phys. Rev. C **46**, 2136(R) (1992).
[29] W. Reviol *et al.*, Acta Phys. Pol. B **30**, 723 (1999).
[30] F. Azaiez *et al.*, Z. Phys. A **338**, 471 (1991).
[31] J. Duprat *et al.*, Phys. Lett. B **341**, 6 (1994).
[32] W. Reviol, D. E. Ellis, L. L. Riedinger, M. P. Carpenter, S. M. Fischer, R. V. F. Janssens, D. Nisius, and P. Fallon, Phys. Rev. C **58**, 2644(R) (1998).
[33] W. Reviol, J. Res. Natl. Inst. Stand. Technol. **105**, 153 (2000).
[34] P. L. Masiteng *et al.*, Phys. Lett. B **719**, 83 (2013).
[35] P. L. Masiteng *et al.*, Eur. Phys. J. A **50**, 119 (2014).
[36] P. L. Masiteng *et al.*, Eur. Phys. J. A **52**, 28 (2016).
[37] J. Ndayishimye *et al.*, Acta Phys. Pol. B **48**, 343 (2017).
[38] J. A. Bounds, C. R. Bingham, P. Juncar, H. K. Carter, G. A. Leander, R. L. Mlekodaj, E. H. Spejewski, and W. M. Fairbank, Phys. Rev. Lett. **55**, 2269 (1985).
[39] J. A. Bounds, C. R. Bingham, H. K. Carter, G. A. Leander, R. L. Mlekodaj, E. H. Spejewski, and W. M. Fairbank, Phys. Rev. C **36**, 2560 (1987).
[40] A. E. Barzakh *et al.*, Phys. Rev. C **95**, 014324 (2017).
[41] S. Das Gupta *et al.*, Phys. Rev. C **88**, 044328 (2013).
[42] J. Ndayishimye, Ph.D. thesis, University of Stellenbosch, 2016.
[43] M. G. Slocombe, J. O. Newton, and G. D. Dracoulis, Nucl. Phys. A **275**, 166 (1977).
[44] H. Pai *et al.*, Phys. Rev. C **88**, 064302 (2013).
[45] D. C. Radford, Nucl. Instrum. Methods A **361**, 297 (1995).
[46] F. Rösel, H. M. Fries, K. Alder, and H. C. Pauli, At. Data Nucl. Data Tables **21**, 291 (1978).
[47] R. M. Diamond and F. S. Stephens, Nucl. Phys. A **45**, 632 (1963).
[48] G. Andersson, E. Arbman, and B. Jung, Ark. Fys. **11**, 297 (1957).
[49] N. Mărginean *et al.*, Eur. Phys. J. A **46**, 329 (2010).
[50] L. Fengying, W. Shuxian, Han Benhua, Weng Peikun, and Y. Chunxiang, Chin. J. Nucl. Phys. **8**, 305 (1986).
[51] A. D. Mehta *et al.*, Z. Phys. A **339**, 317 (1991).
[52] C. Günther, H. Hübel, A. Kleinrahm, D. Mertin, B. Richter, W. D. Schneider, and R. Tischler, Phys. Rev. C **15**, 1298 (1977).
[53] C. Günther *et al.*, Z. Phys. A **301**, 119 (1981).
[54] A. Görgen *et al.*, Eur. Phys. J. A **6**, 141 (1999).
[55] H. Hübel, A. P. Byrne, S. Ogaza, A. E. Stuchbery, G. D. Dracoulis, and M. Guttormsen, Nucl. Phys. A **453**, 316 (1984).
[56] D. Ye *et al.*, Nucl. Phys. A **537**, 207 (1992).
[57] I. G. Bearden *et al.*, Nucl. Phys. A **576**, 441 (1994).
[58] A. Herzáň *et al.*, Phys. Rev. C **96**, 014301 (2017).
[59] H. Pai *et al.*, EPJ Web Conf. **66**, 02079 (2014)
[60] K. H. Hicks, T. E. Ward, J. Wiggins, C. A. Fields, and F. W. N. de Boer, Phys. Rev. C **25**, 2710 (1982).
[61] M. Pfützner *et al.*, Phys. Lett. B **444**, 32 (1998).
[62] J. A. Becker *et al.*, Phys. Rev. C **29**, 1268 (1984).
[63] B. G. Carlsson, I. Ragnarsson, R. Bengtsson, E. O. Lieder, R. M. Lieder, and A. A. Pasternak *et al.*, Phys. Rev. C **78**, 034316 (2008).
[64] T. Bengtsson, Nucl. Phys. A **496**, 56 (1989).
[65] H. L. Ma, B. G. Carlsson, I. Ragnarsson, and H. Ryde, Phys. Rev. C **90**, 014316 (2014).
[66] C. B. Li *et al.*, Phys. Rev. C **94**, 044307 (2016).
[67] L. C. He *et al.*, Chin. Phys. C **41**, 044003 (2017).
[68] T. Bengtsson and I. Ragnarsson, Nucl. Phys. A **436**, 14 (1985).
[69] K. Pomorski and J. Dudek, Phys. Rev. C **67**, 044316 (2003).